Ab initio investigation of the anomalous phonon softening in FeSi

Robin Stern[1] and Georg K. H. Madsen[2,*]
[1]*CMAT, ICAMS, Ruhr-Universität Bochum, 44780 Bochum, Germany*
[2]*Institute of Materials Chemistry, TU Wien, A-1060 Vienna, Austria*
(Received 29 July 2016; published 24 October 2016)

The anomalous softening of the acoustic phonon peak in FeSi has recently received considerable experimental attention. In our work, we investigate the effect of thermal disorder on the lattice dynamics and the filling of the narrow band gap of FeSi using density functional theory. We show, by comparing the phonon density of states from temperature-independent and temperature-dependent force constants, that thermal structural disorder together with thermal expansion explains the anomalously strong renormalization of the acoustic phonons. Furthermore, we find an intricate interplay between thermal disorder and volume in gap closure.

DOI: 10.1103/PhysRevB.94.144304

I. INTRODUCTION

FeSi has received considerable attention since the 1960s [1]. This ongoing research effort is mainly driven by the unusual physical properties and the various provided theories to explain, e.g., the strongly temperature-dependent magnetic susceptibility, the origin and closing of the narrow band gap, and the anomalous phonon softening at elevated temperatures. The magnetic susceptibility follows a Curie-Weiss law for temperatures above 600 K, but goes to zero for 0 K [1]. At low temperatures, FeSi has been found to exhibit a narrow gap of $\varepsilon_g = 0.06$ eV [2,3]. With increasing temperature, the gap becomes smaller and closes around 200–300 K, such that FeSi becomes metallic above room temperature [2,4–8]. Furthermore, the Seebeck coefficient peaks at values between 500–1200 μV/K below 50 K, but is quickly suppressed at higher temperatures [9–13]. These effects are outside what can be expected from a simple temperature broadening of the Kohn-Sham density functional theory [14] (KS-DFT) electronic density of states (DOS). Furthermore, KS-DFT overestimates the gap ($\varepsilon_g^{\mathrm{KS}} \approx 0.12$ eV [15–17]), which is unusual. This would indicate that electron-electron correlations [16] and enhanced spin fluctuations [18] beyond what is included in the single-determinant description have to be considered. Recently, these pictures were reconciled within the dynamical mean-field theory [19,20]. However, thermal disorder has also been used to account for the anomalous temperature-dependent properties of FeSi [17,21,22].

Recently, the phonon properties have also received considerable interest [22–26]. Delaire *et al.* [22,23] and Krannich *et al.* [24] found an anomalous downshift of the acoustic peak in the phonon DOS (pDOS) with increasing temperature, which cannot be explained by thermal expansion alone. Krannich *et al.* link the phonon softening to the unconventional magnetic properties, but also show that the magnetism only appears within KS-DFT after expanding the unit-cell volume to around 100 Å^3 [24]. Delaire *et al.* attribute the softening to the metallization of FeSi above room temperature [22,23]. The explanation of thermal disorder filling the gap was recently challenged by Parshin *et al.* [25]. While they agree on the fact that thermal vibrations do have an influence on the electronic structure, they argue that this does not necessarily lead to a filling of the band gap but can cause the opposite behavior, as, e.g., in the A15 structure V_3Si and V_3Ge [27]. They found that the critical conditions for the metal-to-semiconductor transition lead to similar unit-cell volumes but largely different mean-square displacements (MSD) of the atoms [25].

In this paper, we investigate the origin of the anomalous phonon softening in FeSi using KS-DFT. Two methods for including the effect of temperature on the pDOS are investigated. First, the temperature is only included through the Bose-Einstein (BE) distribution and the quasiharmonic approximation (QHA) where the influence of thermal expansion on the phonon frequencies is taken into account. We furthermore investigate the effect of thermal disorder on the interatomic force constants. This is conceptually different from the usual practice of calculating force constants by sequential displacement of one atom at a time from its equilibrium position [28–31]. The basic idea is that the force constants should reflect the effective potential felt by the atoms at a given temperature. Different implementations of this idea are given in the literature [32–36]. We review the present implementation of the method below. The calculated frequency shifts are compared to published experimental results of the MSD of the atoms and the pDOS. It is shown that the observed phonon softening can be explained from a dynamical point of view if the combination of thermal expansion and disorder is taken into account. Finally, we show that the filling of the gap is not a pure volume effect, but that thermal disorder leads to a renormalization of the electron density of states.

II. METHOD

A. Thermalized displacements

In general, the force on an atom is determined by the displacement of all the atoms in the supercell. From the Taylor expansion of the interatomic potential, V, the force up to second order is given by [37]

$$F_{\alpha_1}^m = -\sum_{n\alpha_2} \phi_{\alpha_1\alpha_2}^{mn} u_{\alpha_2}^n, \tag{1}$$

where ϕ are the second-order force constants, defined as

$$\phi_{\alpha_1\alpha_2}^{mn} = \frac{\partial^2 V}{\partial u_{\alpha_1}^m \partial u_{\alpha_2}^n}. \tag{2}$$

*Corresponding author: georg.madsen@tuwien.ac.at

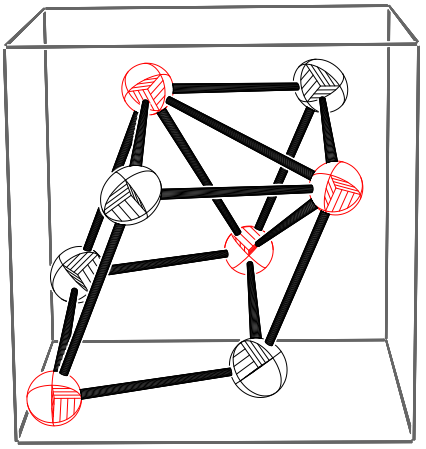

FIG. 1. 99% probability ellipsoid for Fe (red) and Si (black) atoms in FeSi at 750 K. The unit cell was shifted by $1.3 \times (1,1,1)$ Å with respect to the crystallographic unit cell. Figure created with ORTEP-III. [39]

The α's indicate the direction, m and n are the atom indices, u are the displacements of the atoms from their equilibrium position, and F is the resulting forces. In a perfectly harmonic potential, the force constants obtained from inverting Eq. (1) are obviously independent of the displacements used.

The idea of using thermalized displacements is to generate an effective force field corresponding to the average potential felt at a given temperature. In the case of thermal disorder, all elements of u_α^m are nonzero, so that all atoms in the supercell are displaced from their equilibrium position. To obtain the thermalized displacements, we start with the MSD matrix of atom l, which is given as [38]

$$\langle u_l^2 \rangle = \frac{1}{N m_l} \sum_{j\mathbf{q}} \frac{E_{j\mathbf{q}}}{\omega_{j\mathbf{q}}^2} \mathbf{e}_{j\mathbf{q}}(l) \mathbf{e}_{j\mathbf{q}}^\dagger(l), \tag{3}$$

where N is the number of $\mathbf{q}$ points, m_l is the mass of atom l, and $\omega_{j\mathbf{q}}$ and $\mathbf{e}_{j\mathbf{q}}$ are, respectively, the frequency and polarization vector of mode j at point $\mathbf{q}$ in the Brillouin zone. The average energy of mode $j\mathbf{q}$,

$$E_{j\mathbf{q}} = \hbar\omega_{j\mathbf{q}}\left(\eta_{j\mathbf{q}} + \tfrac{1}{2}\right), \tag{4}$$

is temperature dependent through the BE distribution $\eta_{j\mathbf{q}}$. The matrix $\langle u_l^2 \rangle$ determines the probability distribution of the atoms [38],

$$p_l(\mathbf{u}) = \sqrt{\frac{\det\left(\langle u_l^2 \rangle^{-1}\right)}{8\pi^3}} \exp\left(-\frac{\mathbf{u}^T \langle u_l^2 \rangle^{-1} \mathbf{u}}{2}\right). \tag{5}$$

Based on the probability distribution function (PDF), given by Eq. (5), of a given atom, ellipsoids of equal probability can be defined (Fig. 1). They depend on temperature directly through the BE distribution and indirectly through the volume dependence and displacement dependence of the frequencies.

Getting volume- and displacement-dependent force constants is schematically illustrated in Fig. 2. First, the volume-dependent force constants are calculated at volumes within ±2% using finite displacements. From these volume-dependent but nonthermalized force constants, we get the temperature-volume curve by minimizing the free energy at each temperature. For each volume, the $\langle u_l^2 \rangle$'s, given by Eq. (3), are then calculated using the temperature corresponding to that given volume. To obtain a set of thermalized displacements, we draw random samples from the probability distribution defined by Eq. (5) and obtain new force constants with the algorithm described below. The obtained force constants and resulting phonon frequencies thus depend on the displacements, which in turn depend on the phonon frequencies. This leads to a self-consistent procedure (Fig. 2), which can be repeated until the MSD no longer change. Alternatively, the temperature-volume curve can be obtained from experiment, where the rest of the procedure remains the same.

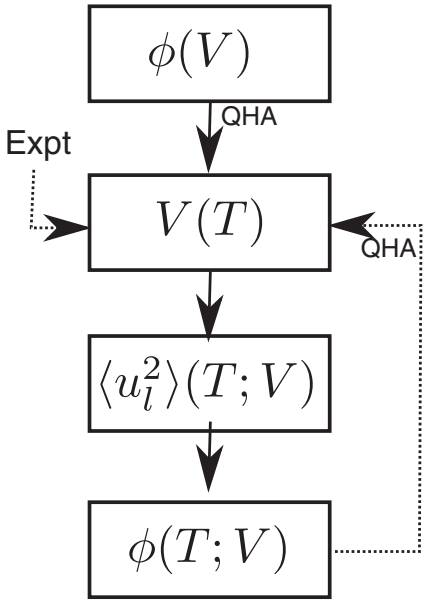

FIG. 2. Outline of the calculation procedure.

B. Force constants

In principle, the force constants can be determined by obtaining forces for $3N$ sets of displacements and inverting Eq. (1). However, these will not obey crystal symmetry and, even for an overdetermined system, a very slow convergence is observed. It is therefore necessary to introduce symmetry explicitly in the optimization procedure. To do this, it is computationally convenient to rewrite Eq. (1) in a vectorized form [29,33,40],

$$\mathbf{F}_m = -\sum_n \tilde{u}_n \phi^{mn}, \tag{6}$$

where

$$\phi^{mn} = \begin{pmatrix} \phi_{xx}^{mn} \\ \phi_{xy}^{mn} \\ \phi_{xz}^{mn} \\ \vdots \\ \phi_{zz}^{mn} \end{pmatrix}. \tag{7}$$

The displacements are rewritten as

$$\tilde{u}_n = \mathbb{1} \otimes \left(u_x^n, u_y^n, u_z^n\right), \tag{8}$$

which results in a 3×9 dimensional matrix.

Symmetry makes it possible to reduce the number of independent force constants. From Eq. (2), it follows that the force constant tensors are symmetric, i.e.,

$$\phi^{mn}_{\alpha_1\alpha_2} = \phi^{nm}_{\alpha_2\alpha_1}. \tag{9}$$

Further, if a space-group operation S with the rotation matrix R maps atoms n and m onto $S(n)$ and $S(m)$, then the force constants can be expressed as

$$\phi^{S(m)S(n)} = \tilde{R}\phi^{mn}, \tag{10}$$

where $\tilde{R}$ is the rotation operation rewritten as a 9×9 matrix to match the vectorized form of the force constant matrix ϕ, given by Eq. (7). Considering the constraints following from Eqs. (9) and (10), it is possible to reduce the problem such that

$$\mathbf{F} = C(\tilde{u})\boldsymbol{\varphi}, \tag{11}$$

where $\mathbf{F}$ is the $3N\nu$-dimensional force vector, N is the number of atoms, ν is the number of force fields, and C is a matrix containing the linear combinations of displacements due to symmetry [33]. C has the dimensions $3N\nu \times N_{\mathrm{IFC}}$, where N_{IFC} is the number of independent force constants. $\boldsymbol{\varphi}$ is a vector containing the independent force constants.

Translational and rotational invariance is included via the acoustic

$$0 = \sum_n \phi^{mn}_{\alpha_1\alpha_2} \tag{12}$$

and rotational sum rules [37]

$$0 = \sum_n \phi^{mn}_{\alpha_1\alpha_2} x^{mn}_{\alpha_3} - \phi^{mn}_{\alpha_1\alpha_3} x^{mn}_{\alpha_2}, \tag{13}$$

where $x^{mn}_{\alpha} = x^{m}_{\alpha} - x^{n}_{\alpha}$. We implement these rules using the vectorized notation given by Eqs. (7) and (8) by including extra displacements. For the translational invariance, there are displacements of all atoms along the three Cartesian coordinates, such that

$$\tilde{u}^{x,\mathrm{ti}}_n = \mathbb{1} \otimes (1\,0\,0), \tag{14}$$

$$\tilde{u}^{y,\mathrm{ti}}_n = \mathbb{1} \otimes (0\,1\,0), \tag{15}$$

$$\tilde{u}^{z,\mathrm{ti}}_n = \mathbb{1} \otimes (0\,0\,1). \tag{16}$$

For rotational invariance, each mn pair defines the matrix

$$\tilde{u}^{\mathrm{ri}}_{mn} = \begin{pmatrix} 0 & -x^{mn}_z & x^{mn}_y & 0 & 0 & 0 & 0 & 0 & 0 \\ 0 & 0 & 0 & x^{mn}_z & 0 & -x^{mn}_x & 0 & 0 & 0 \\ 0 & 0 & 0 & 0 & 0 & 0 & x^{mn}_y & -x^{mn}_x & 0 \end{pmatrix}. \tag{17}$$

The force constants can then be calculated by inverting the C matrix,

$$\mathbf{F} = \begin{pmatrix} C(\tilde{u}) \\ C(\tilde{u}^{\mathrm{ti}}) \\ C(\tilde{u}^{\mathrm{ri}}) \end{pmatrix} \boldsymbol{\varphi}, \tag{18}$$

where $C(\tilde{u}^{\mathrm{ti}})$ and $C(\tilde{u}^{\mathrm{ri}})$ are the symmetry-reduced rotational and translational displacements. The $\mathbf{F}$ components corresponding to the $\tilde{u}^{\mathrm{ti}}$ and $\tilde{u}^{\mathrm{ri}}$ displacements are zero. Since the extra displacements for translational and rotational invariance do not enforce the exact fulfillment of the invariance conditions, it is possible to multiply a specific weight to $C(\tilde{u}^{\mathrm{ti/ri}})$. This gives control over how well the conditions, given by Eqs. (12) and (13), are to be satisfied at the cost of reproducing the force fields. To obtain a converged result, the system of linear equations is overdetermined and the independent force constants are found using singular-value decomposition of C.

III. COMPUTATIONAL DETAILS

We conducted DFT calculations using VASP [41]. As exchange correlation functional, we used the generalized gradient approximation Perdew-Burke-Ernzerhof (PBE) [42]. The calculations to get the force constants from finite displacements as well as from thermal disorder were done in a $2 \times 2 \times 2$ orthogonal supercell containing 64 atoms with a $5 \times 5 \times 5$ Monkhorst-Pack k mesh with an energy cutoff of 500 eV. The electron DOS was calculated in two steps. First, the charge density in the supercell with thermal disorder was calculated with a $5 \times 5 \times 5$ Monkhorst-Pack k mesh. Second, after achieving self-consistency, the charge density was fixed and the DOS was calculated on a fine $11 \times 11 \times 11k$ mesh with a cutoff energy of 270 eV. The sequential displacements were generated by displacing the atoms by 0.01 Å one at a time from their equilibrium position. We used 25 thermalized sets of displacements generated according to the thermal PDF, given by Eq. (5). The symmetry operators used for the generation of the C matrix were taken from spglib [43].

IV. RESULTS AND DISCUSSION

Figure 3 shows the phonon band structure and pDOS for the DFT equilibrium volume with nonthermalized force constants (black line). The phonon band structures 750 K QHA volume

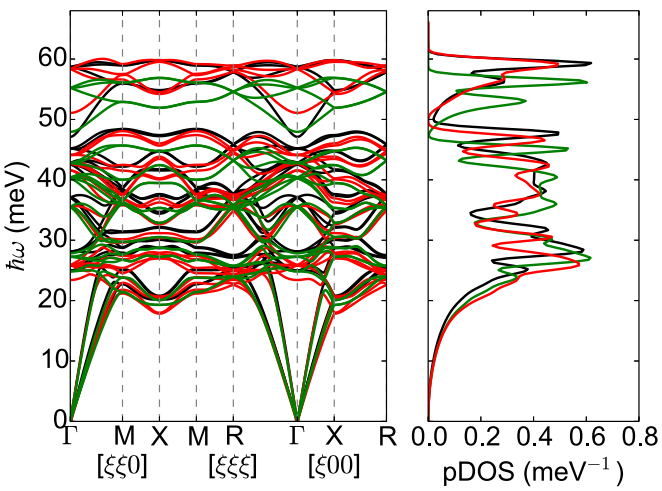

FIG. 3. FeSi phonon band structure and density of states. Black: PBE equilibrium volume and force constants from sequential displacements. Green: $V_{\mathrm{QHA}}(750\,\mathrm{K})$ nonthermalized force constants from sequential displacements. Red: $V_{\mathrm{QHA}}(750\,\mathrm{K})$ thermalized force constants corresponding to 750 K. The density of states have been normalized to the number of atoms in the unit cell.

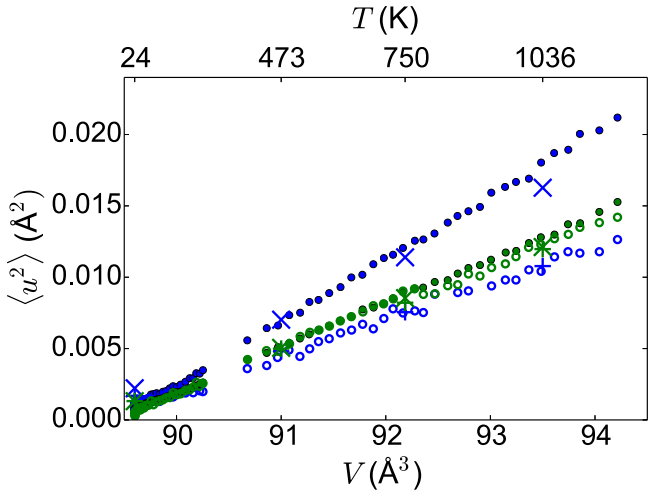

FIG. 4. MSD along the principal axes of the equal probability ellipsoids. Full circles and crosses correspond to $\langle u_{11}^2 \rangle$. Open circles and plus signs correspond to $\langle u_{33}^2 \rangle$. Circles show experimental values taken from Ref. [44]. Green corresponds to iron and blue corresponds to Si. Crosses and plus signs are calculated from thermalized force constants obtained at four volumes using the experimental temperatures (upper x axis) corresponding to these volumes.

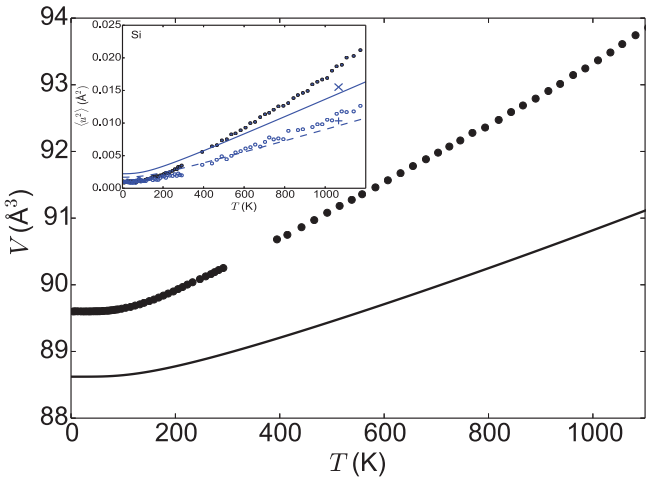

FIG. 5. Experimental volume-temperature curve [44] (dots) and calculated with QHA (solid line). The inset shows the MSD of Si calculated using the QHA volume at the given temperature.

(90.0 Å^3) using force constants obtained from finite sequential displacements (green line) are also shown. It is clear that a shift of the acoustic peak occurs due to the volume expansion. The shift is about 5.2%. This is more than what would be estimated from volume change alone using a Grüneisen parameter of $\gamma = 1.6$, as done earlier [23], but still substantially less than the shift of 14% reported experimentally [23,24].

To investigate the role of thermal disorder, we then calculated thermalized force constants at the volume of 90.0 Å^3 using a temperature of 750 K to generate the MSD. Thereby a further shift of 4.5% of the main acoustic peak (red line in Fig. 3) compared to the results obtained with the sequential displacements occurs. This brings the total shift of 9.7% into better agreement with experiment and underlines that increasing thermal disorder with increasing temperature affects the force constants substantially and plays a role in explaining the phonon DOS at elevated temperatures.

The MSD used for determining the thermalized displacements can be validated by comparison to those obtained from the refinement of diffraction data. The MSD obtained for FeSi from experimental data [44] are shown in Fig. 4. For Si, an anisotropy is clearly seen, which is in accordance with the point group of the atomic position. FeSi crystallizes in a cubic B-20 structure (space group 198) with 8 atoms per unit cell [45]. In FeSi, the atoms occupy the Wyckoff position a. This leads to a MSD matrix with two independent coefficients [38],

$$\langle u_l^2 \rangle = \begin{pmatrix} A & B & B \\ B & A & B \\ B & B & A \end{pmatrix}, \tag{19}$$

where A and B are different for Fe and Si atoms. The MSD matrix, given by Eq. (19), will give two distinct principle axes of the equal probability ellipsoid (Fig. 1). We have calculated the MSD from thermalized force constants at four volumes using the corresponding experimental temperature (upper x axis in Fig. 4). The anisotropy and magnitude of both the Si and Fe MSDs are very well recovered and agree quantitatively with experiment, even at high temperatures. It is thus clear that the MSDs are well described by volume-dependent force constants. The importance of taking the volume dependence of the force constants into account is underlined if we fix the force constants to those obtained at a unit-cell volume of 89.6 Å^3 and include temperature only in the BE distribution. The obtained MSD, shown in the inset in Fig. 5 as solid lines, significantly underestimates the experimental MSD at high temperatures. Force constants were obtained for the four volumes using both sequential and thermal displacements. However, the difference was found to be very small. For example, at 750 K, the MSDs from sequential force constants and the corresponding thermalized force constants $\langle u_{\mathrm{Si},11}^2 \rangle$ differ less than 10^{-5} Å^2. This underlines that the MSDs are not sensitive to the displacements used, as opposed to the frequencies (Fig. 3). We have therefore not taken further iterations of the self-consistent procedure illustrated in Fig. 2.

An alternative to using the experimental temperature-volume curve is to calculate it directly from the QHA (see scheme in Fig. 2). The hereby obtained curve is shown in Fig. 5. The calculation clearly underestimates the unit-cell volume. The relaxed cell has a unit-cell volume of 88.1 Å^3, which underestimates the low-temperature experimental result of 89.6 Å^3 by about 1.7% [44]. Including zero-point vibrations increases the calculated volume to 88.6 Å^3, which is still approximately 1% lower than the experimental result. The influence of the underestimated unit-cell volume on the calculated MSDs is illustrated in Fig. 5 (inset). The calculated MSDs (crosses at 1066 K) are underestimated due to the underestimated unit-cell volume (calculated to 91.0 Å^3 instead of the experimental 93.7 Å^3 at 1000 K). In a direct comparison with experiment, the QHA for FeSi thus introduces a bias. For a given volume, it leads to an overestimated temperature or, for a given temperature, leads to an underestimated unit-cell volume.

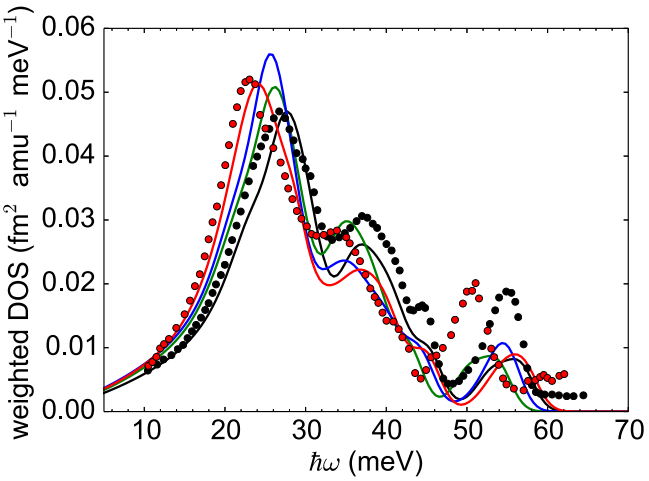

FIG. 6. Weighted phonon DOS of FeSi. Black: $V_{\text{exp}}(0\text{ K})$ and nonthermalized force constants. Green: $V_{\text{exp}}(750\text{ K})$ and nonthermalized force constants. Blue/red: $V_{\text{exp}}(750\text{ K})$ and using thermalized force constants evaluated at 750 and 1250 K. The calculated projected phonon DOS is weighted with the coherent scattering lengths, 4.15 and 9.45 fm, and masses, 28.09 and 55.85 amu, for Si and Fe, respectively [46]. A Gaussian smearing of $\sigma = 0.4$ was used. The intensity was scaled to the 10 K low-temperature experimental acoustic peak. The same scaling was then applied to all the calculated phonon DOS. The experimental data are taken from Ref. [23].

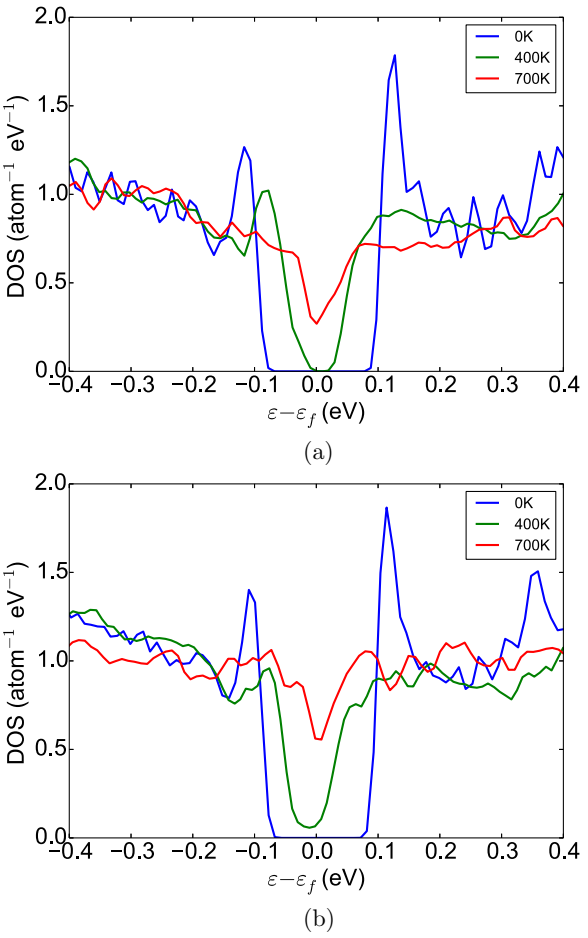

FIG. 7. Electron density of states for FeSi at (a) $0.94 \times V_0$ and (b) V_0. For each temperature, the DOS of two sets of thermal disordered structures were calculated and averaged. The label corresponds to the temperature used to generate the thermalized displacements.

The results discussed above underline two points. First of all, the position of the phonon peaks is sensitive to the displacements used to obtain the force constants. Second, there is a certain bias in the QHA temperature-volume curve which prevents the theory from being fully quantitative.

To further analyze the dependence of the phonon peaks on the displacements used, we have calculated the weighted phonon DOS of FeSi for comparison with experiment (Fig. 6). The effect of volume expansion on the phonon DOS without temperature effects is comparable to the shift that occurs in the QHA (Fig. 3). Expanding the volume from $V_{\text{expt}}(0\text{ K})$ (black line) to $V_{\text{expt}}(750\text{ K})$ (green line) leads to a downward shift of the main peak of about 5.7% (Fig. 6). Calculating the pDOS from the 750 K thermalized displacements results in a further shift of 2.5%, such that the total shift is 8.2%. Increasing the temperature used to generate the thermal displacements to 1250 K but keeping the volume fixed yields a significant total shift of the acoustic peak of 14.5% (red line, Fig. 6). It should be noted that the relative position of the calculated 0 K peak is slightly shifted to higher frequencies, which explains why the high-temperature peak does not exactly match the experimental peak position even though there is a 14% shift.

It is thus possible to obtain a very good agreement between the experimental and calculated shift of the main peak, although with an MSD evaluated at a higher temperature. This falls in line with an overbinding of the functional indicated by the underestimated lattice constant. Overbinding within the PBE functional, which otherwise tends to overestimate unit-cell volume, is unusual [47,48]. It can be related to self-interaction error, which will tend to make the d orbitals more bandlike. The overbinding could be corrected using a self-interaction corrected or "$+U$"-like scheme [49]. This would, however, further open the already overestimated band gap. In this context, it is interesting that PBE also underestimates the lattice constant of FeAl [48], which is another compound that has been discussed in the context of electron-electron correlations [50]. As such, our results provide further evidence that for a quantitative theory for FeSi, it is necessary to include electron-electron correlations beyond the single-determinant KS-DFT description. Furthermore, they underline that thermal disorder plays an important role in the high-temperature properties.

Finally, we will discuss the role of the gap filling and metallization in the anomalous temperature dependence of the acoustic peak. We calculated the electron DOS of FeSi for two different volumes (Fig. 7). The curves labeled 0 K are obtained with the atoms at their equilibrium positions. The curves labeled 400 and 700 K were calculated by displacing the atoms according to the PDF, given by Eq. (5), and averaging the DOS obtained for two different thermally disordered supercells. The results in Fig. 7 show that regardless of the volume, ordered FeSi exhibits a band gap of about 120 meV. Thermal disorder closes the band gap, where the critical temperature for smaller volumes is higher than for higher volumes. For the small volume, the critical temperature is between 400 and 700 K,

whereas for the large volume, the gap closes between 0 and 400 K. Our results agree with the measurements of Parshin *et al.* [25], who found that the MSD at the critical conditions for pressure and temperature can be significantly different.

We notice that at equilibrium volume and thermal disorder corresponding to 700 K, the band gap is closed (see Fig. 7). However, as opposed to the 750 K QHA volume, we find no significant shift of the acoustic peak when using the 750 K thermalized force constants. If the metallization of FeSi, which is driven by structural disorder, would cause the shifting of the low-frequency peaks, then we should see it at both the equilibrium volume and 750 K. Thus, the origin of the anomalous downshift is not so much the metallization of the material, but rather the increasing importance of anharmonicity in the potential energy landscape with increasing volume. The filling of the band gap is thus caused by structural disorder. However, the filling of the gap itself does not influence the anomalous softening of the phonons.

V. CONCLUSION

We have found that volume expansion contributes a significant part to the phonon softening in FeSi. However, the anomalously large softening of the acoustic peak can only be explained by the combination of volume expansion and the effect of thermal disorder on the interatomic bonding. The PBE is found to overbind and underestimate the unit-cell volume.

Our results indicate that both electron-electron correlation beyond the single-determinant KS description as well as thermal disorder play important roles for the high-temperature properties of FeSi. As such, our results fall in line with the conclusions by Tomczak *et al.* and Kunes *et al.* [19,20], who showed how FeSi is moderately correlated but has an electronic structure where these moderate correlations are essential for a correct description.

We calculated the mean-square displacements of Si and Fe atoms in FeSi from temperature-dependent force constants at experimental volumes and achieved very good agreement with reported results. A pure volume effect of closing the gap can be excluded from the theoretical point of view, since the band gap was not found to change with volume. However, thermal disorder leads to a closing of the gap and the critical temperatures differ for the three considered volumes. While thermal disorder plays a crucial role in explaining the filling of the gap and the anomalous phonon softening, the metallization of FeSi does not lead to a considerable phonon softening at equilibrium volume.

ACKNOWLEDGMENT

We acknowledge support from M-era.net through the ICETS Project No. DFG: MA 5487/4-1.

[1] V. Jaccarino, G. K. Wertheim, J. H. Wernick, L. R. Walker, and S. Arajs, Phys. Rev. **160**, 476 (1967).
[2] Z. Schlesinger, Z. Fisk, H.-T. Zhang, M. B. Maple, J. DiTusa, and G. Aeppli, Phys. Rev. Lett. **71**, 1748 (1993).
[3] L. Degiorgi, M. B. Hunt, H. R. Ott, M. Dressel, B. J. Feenstra, G. Grüner, Z. Fisk and P. Canfield, Europhys. Lett. **28**, 341 (1994).
[4] A. Chainani, T. Yokoya, T. Morimoto, T. Takahashi, S. Yoshii, and M. Kasaya, Phys. Rev. B **50**, 8915 (1994).
[5] T. Saitoh, A. Sekiyama, T. Mizokawa, A. Fujimori, K. Ito, H. Nakamura, and M. Shiga, Solid State Commun. **95**, 307 (1995).
[6] S. Paschen, E. Felder, M. A. Chernikov, L. Degiorgi, H. Schwer, H. R. Ott, D. P. Young, J. L. Sarrao, and Z. Fisk, Phys. Rev. B **56**, 12916 (1997).
[7] K. Breuer, S. Messerli, D. Purdie, M. Garnier, M. Hengsberger, Y. Baer, and M. Mihalik, Phys. Rev. B **56**, R7061(R) (1997).
[8] K. Ishizaka, T. Kiss, T. Shimojima, T. Yokoya, T. Togashi, S. Watanabe, C. Q. Zhang, C. T. Chen, Y. Onose, Y. Tokura, and S. Shin, Phys. Rev. B **72**, 233202 (2005).
[9] R. Wolfe, J. Wernick, and S. Haszko, Phys. Lett. **19**, 449 (1965).
[10] B. C. Sales, E. C. Jones, B. C. Chakoumakos, J. A. Fernandez-Barca, H. E. Harmon, and J. W. Sharp, Phys. Rev. B **50**, 8207 (1994).
[11] B. Buschinger, C. Geibel, F. Steglich, D. Mandrus, D. Young, J. Sarrao, and Z. Fisk, Physica B: Condens. Matter **230–232**, 784 (1997).
[12] N. E. Sluchanko, V. V. Glushkov, S. V. Demishev, M. V. Kondrin, K. M. Petukhov, N. A. Samarin, V. V. Moshchalkov, and A. A. Menoskyv, Europhys. Lett. **51**, 557 (2000).
[13] B. C. Sales, O. Delaire, M. A. McGuire, and A. F. May, Phys. Rev. B **83**, 125209 (2011).
[14] W. Kohn and L. J. Sham, Phys. Rev. **140**, A1133 (1965).
[15] L. F. Mattheiss and D. R. Hamann, Phys. Rev. B **47**, 13114 (1993).
[16] C. Fu and S. Doniach, Phys. Rev. B **51**, 17439 (1995).
[17] T. Jarlborg, Phys. Rev. B **59**, 15002 (1999).
[18] Y. Takahashi, J. Phys.: Condens. Matter **9**, 2593 (1997).
[19] J. Kuneš and V. I. Anisimov, Phys. Rev. B **78**, 033109 (2008).
[20] J. M. Tomczak, K. Haule, and G. Kotliar, Proc. Natl. Acad. Sci. USA **109**, 3243 (2012).
[21] T. Jarlborg, Phys. Rev. B **76**, 205105 (2007).
[22] O. Delaire, I. I. Al-Qasir, J. Ma, A. M. dos Santos, B. C. Sales, L. Mauger, M. B. Stone, D. L. Abernathy, Y. Xiao, and M. Somayazulu, Phys. Rev. B **87**, 184304 (2013).
[23] O. Delaire, K. Marty, M. B. Stone, P. R. C. Kent, M. S. Lucas, D. L. Abernathy, D. Mandrus, and B. C. Sales, Proc. Natl. Acad. Sci. USA **108**, 4725 (2011).
[24] S. Krannich, Y. Sidis, D. Lamago, R. Heid, J.-M. Mignot, H. v. Loehneysen, A. Ivanov, P. Steffens, T. Keller, L. Wang, E. Goering, and F. Weber, Nat. Commun. **6**, 8961 (2015).
[25] P. P. Parshin, A. I. Chumakov, P. A. Alekseev, K. S. Nemkovski, J. Perßon, L. Dubrovinsky, A. Kantor, and R. Rüffer, Phys. Rev. B **93**, 081102(R) (2016).
[26] Y. S. Ponosov, A. O. Shorikov, S. V. Streltsov, A. V. Lukoyanov, N. I. Shchegolikhina, A. F. Prekul, and V. I. Anisimov, JETP Lett. **103**, 316 (2016).
[27] O. Delaire, M. S. Lucas, J. A. Muñoz, M. Kresch, and B. Fultz, Phys. Rev. Lett. **101**, 105504 (2008).

[28] W. Frank, C. Elsässer, and M. Fähnle, Phys. Rev. Lett. **74**, 1791 (1995).
[29] K. Parlinski, Z. Q. Li, and Y. Kawazoe, Phys. Rev. Lett. **78**, 4063 (1997).
[30] K. Esfarjani and H. T. Stokes, Phys. Rev. B **77**, 144112 (2008).
[31] A. Togo, L. Chaput, and I. Tanaka, Phys. Rev. B **91**, 094306 (2015).
[32] P. Souvatzis, O. Eriksson, M. I. Katsnelson, and S. P. Rudin, Phys. Rev. Lett. **100**, 095901 (2008).
[33] O. Hellman, P. Steneteg, I. A. Abrikosov, and S. I. Simak, Phys. Rev. B **87**, 104111 (2013).
[34] I. Errea, M. Calandra, and F. Mauri, Phys. Rev. Lett. **111**, 177002 (2013).
[35] F. Zhou, W. Nielson, Y. Xia, and V. Ozoliņš, Phys. Rev. Lett. **113**, 185501 (2014).
[36] T. Tadano and S. Tsuneyuki, Phys. Rev. B **92**, 054301 (2015).
[37] M. Born and K. Huang, *Dynamical Theory of Crystal Lattices* (Clarendon, Oxford, 1998).
[38] B. T. M. Willis and A. W. Pryor, *Thermal Vibrations in Crystallography* (Cambridge University Press, Cambridge, 1975).
[39] L. J. Farrugia, J. Appl. Crystallogr. **45**, 849 (2012).
[40] L. Chaput, A. Togo, I. Tanaka, and G. Hug, Phys. Rev. B **84**, 094302 (2011).
[41] G. Kresse and J. Furthmüller, Phys. Rev. B **54**, 11169 (1996).
[42] J. P. Perdew, K. Burke, and M. Ernzerhof, Phys. Rev. Lett. **77**, 3865 (1996).
[43] A. Togo, *spglib, a C library for finding and handling crystal symmetries*, http://spglib.sourceforge.net/ (unpublished).
[44] L. Vočadlo, S. K. Knight, D. G. Price, and G. I. Wood, Phys. Chem. Miner. **29**, 132 (2002).
[45] I. G. Wood, W. I. F. David, S. Hull, and G. D. Price, J. Appl. Crystallogr. **29**, 215 (1996).
[46] *Neutron scattering lengths*, https://www.ncnr.nist.gov/resources/n-lengths/ (unpublished).
[47] G. K. H. Madsen, Phys. Rev. B **75**, 195108 (2007).
[48] P. Haas, F. Tran, and P. Blaha, Phys. Rev. B **79**, 085104 (2009).
[49] J. P. Perdew, R. G. Parr, M. Levy and J. L. Balduz, Jr, Phys. Rev. Lett. **49**, 1691 (1982).
[50] A. G. Petukhov, I. I. Mazin, L. Chioncel, and A. I. Lichtenstein, Phys. Rev. B **67**, 153106 (2003).